Environmental
Science
Nano

ROYAL SOCIETY
OF CHEMISTRY

Wrinkle-Induced High Sorption Makes Few-layered Black Phosphorus a Superior Adsorbent for Ionic Organic Compounds

SCHOLARONE™
Manuscripts

Environmental significance

Developing new adsorbents with high adsorption capacities for ionic organic compounds (IOCs) is essential to effectively remove IOCs from aqueous solution. Although black phosphorus (BP) has been applied in electronics, photonics, and photothermal/photodynamic therapies in biomedical research, its application for IOCs removal from the environment has not been reported yet. Inspired by the high drug loading capacity of black phosphorus (BP), we here report that the few-layered BP has high adsorption capacities for both cationic methylene blue (1232 ± 283 mg/g) and anionic congo red (230 ± 9 mg/g), these values are among the highest capabilities reported. The wrinkle-induced sorption mechanism was demonstrated by TEM and AFM analysis, and was verified via DFT calculation to account for the high adsorption capacities.

1　# Wrinkle-Induced High Sorption Makes Few-layered

2　# Black Phosphorus a Superior Adsorbent for Ionic

3　# Organic Compounds

4　Qing Zhao,†[a] Wei Ma,†[a,b] Bo Pan,[c] Qianru Zhang, [a] Xuejiao Zhang,*[a] Siyu Zhang,*[a.d] Baoshan

5　Xing*[d]

6

7　[a] Key Laboratory of Pollution Ecology and Environmental Engineering Institute of Applied

8　Ecology, Chinese Academy of Sciences, Shenyang 110016, China. Email:

9　zhangxuejiao@iae.ac.cn (Xuejiao Zhang); syzhang@iae.ac.cn (Siyu Zhang)

10　[b] University of Chinese Academy of Sciences Chinese Academy of Sciences Beijing 100049,

11　China

12　[c] Faculty of Environmental Science & Engineering, Kunming University of Science &

13　Technology, Kunming 650500, China

14　[d] Stockbridge School of Agriculture University of Massachusetts, Amherst, Massachusetts

15　01003, USA. E-mail: bx@umass.edu; Fax: +413 577 0242; Tel: +413 545 5212

16

17

18

19

20   **Abstract**

21   There is a challenge in effectively removing ionic organic compounds from aqueous solution.

22   Inspired by the high drug loading capacity of black phosphorus (BP), we here show that the few-

23   layered BP has high adsorption capacities for both cationic methylene blue (1232 ± 283 mg/g)

24   and anionic congo red (230 ± 9 mg/g), these values are among the highest capabilities reported.

25   The maximum theoretical specific surface area of single layered BP is calculated to be 2400 m^2/g

26   for the first time. Both electrostatic and hydrophobic interactions are responsible for methylene

27   blue sorption on BP, whereas hydrophobic interactions are the main force for congo red sorption.

28   Sorption kinetic study indicates the intraparticle diffusion mechanism was involved in both dyes

29   sorption. Most importantly, the wrinkle-induced sorption mechanism was demonstrated by TEM

30   and AFM analysis, and was verified via DFT calculation to account for the high adsorption

31   capacities. These findings demonstrate the promising use of BP as an innovative adsorbent for

32   IOCs in environmental management.

33

34

35

36

37

38

39

40

41

42

43

44

INTRODUCTION

There are increasing concerns over the global occurrence of organic pollutants in water, such as dyes, antibiotics, herbicides, endocrine disrupting compounds and personal care products, because they cause a series of ecological problems and threaten human health.[1-3] Many of these pollutants are ionic at environmentally relevant pH.[4] Great efforts have been made on the efficient removal of ionic organic compounds (IOCs) by adsorption techniques, because of the preconcentration and solidification of IOCs on adsorbents.[5] However, compared to non-ionic compounds,[6, 7] until now it is still a challenge to effectively adsorb IOCs from aqueous solution, due to their high water solubility. Therefore, it is essential to develop new adsorbents with high adsorption capacities for IOCs.

As a rising star of post-graphene two-dimensional (2D) nanomaterials, black phosphorus (BP) has gained more and more attentions since 2014.[8] Due to the remarkable properties of few-layered BP, it has been applied in electronics,[9-11] photonics,[10, 12, 13] and photothermal/photodynamic therapies in biomedical research.[14, 15] Recently, few-layered BP has been explored to serve as a drug delivery platform.[16, 17] Polyethylene glycol-modified BP showed a superior sorption capacity of 1080 mg/g for doxorubicin (DOX) and 304 mg/g for Cyanine7, higher than most of the reported delivery systems with loading capacities ranging from 100 to 300 mg/g.[16] Meanwhile, a recent report claimed that n-methylpyrrolidone exfoliated BP exhibited an incredible loading capacity of 9500 mg/g, the highest to date.[17] Although the above findings suggest the organic solvents modified/exfoliated-BP as a promising adsorbent for IOCs, the sorption ability of pure layered BP is still unknown. Since organic solvents will compete sorption sites with IOCs on BP surface, pure layered BP will display a higher sorption ability than organic solvents modified/exfoliated-BP. Also, application of few-layered BP for IOCs

68   removal from the environment has not been reported yet. In addition, the mechanisms of sorption

69   are still unclear.

70   In this work, we exfoliated bulk BP single crystals directly in the oxygen-free Mill-pore water

71   by ultrasonication to obtain the few-layered BP. Sorption of two model IOCs, a cationic dye

72   methylene blue (MB) and an anionic dye congo red (CR) (Figure S1, Supplementary

73   Information), by few-layered BP were systematically studied. Via a combination of sorption

74   isotherm models, sorption kinetics, density functional theory (DFT) calculation, and optical

75   microscopy, the sorption mechanism was disclosed. The maximum theoretical specific surface

76   area of single BP layer was calculated for the first time. The few-layered BP displayed excellent

77   sorption capacities for both dyes. Therefore, our study demonstrated the promising potential of

78   few-layered BP for the effective removal of IOCs from aqueous solution, which will likely

79   expand its environmental application in the future.

80   **EXPERIMENTAL SECTION**

81   **Materials**

82   BP crystals (purity >99.998%) were bought from Nanjing XF NANO Materials Tech Co., Ltd.

83   MB (purity 99.5%) was purchased from Beijing J&K Scientific Ltd. CR (purity > 98.0%) was

84   obtained from Tokyo Chemical Industry Co., Ltd. Ultrapure water was obtained with a

85   Millipore- Milli Q system.

86   **Exfoliation procedure of few-layered BP**

87   Few-layered BP was prepared by direct ultrasonication in Milli-pore water. The bulk BP

88   crystals were gradually ground into BP powders with an agate mortar in the glove box. After

89   being transferred to a 40 mL sealed anaerobic bottle containing 35 mL oxygen-free Milli-pore

90   water, the BP powders were ultrasonicated using an ultrasonic cell disruption system (JY 88-IIN)

91   for 12 h at the power of 75 W. Ice bath was used during the whole process to keep the

92   temperature below 10 °C. Finally, the suspension was centrifuged at 100 g for 20 min to separate

93   the precipitate of un-exfoliated BP crystals and the supernatant of few-layered BP for the further

94   experiments.

95   **Characterizations**

96   In order to determine the concentration of few-layered BP suspension, inductively coupled

97   plasma optical emission spectroscopy (ICP-OES, Agilent 5100) was used to determine the

98   phosphorus content after diluting the BP suspension. The thickness and lateral size of few-

99   layered BP before and after adsorption of dyes were examined by tapping mode AFM (Agilent

100   5100) in ambient condition. The BP suspension was dropped onto Si substrate, which was dried

101   under inert atmosphere in the glove box before AFM measurements. The morphological

102   transformation of few-layered BP before and after sorption was characterized by TEM equipped

103   with an FEI Tecnai F20, operated at 200 kV. Raman spectroscopy and XPS measurements were

104   performed to evaluate the crystalline structure and chemical purity of few-layered BP,

105   respectively. Raman spectra were recorded by a Thermo scientific DXR Raman Microscope with

106   a CCD detector and a 780 nm laser line at 24 mW. XPS measurements were carried out using

107   ESCALAB250 (Thermo VG) with a monochromated A1 Kα X-ray source at 1486.6 eV. The dye

108   concentrations after adsorption was quantified by a UV spectrophotometer (Shimadzu, UV-2700)

109   at characteristic absorptions of 664 and 494 nm for MB and CR, respectively. Zetasizer Nano ZS

110   (Marvern Instruments) equipped with a He-Ne laser source was used to measure the

111   hydrodynamic diameter and zeta potential of few-layered BP suspension. The structural stability

112   of dyes in the process of adsorption by few-layered BP were examined by HPLC (Agilent 1260).

1
2
3   **Sorption experiments**
4
113
5
6   Sorption experiments were performed using a batch equilibration technique under anaerobic
7
114
8
9   conditions. Briefly, 2 mL BP suspension was mixed with 8 mL background solution (pH 7.0,
10
115
11   0.01 M Na$^+$ PBS buffer, 200 mg/L NaN$_3$) with different initial concentration of dyes (for sorption
12
116
13   isotherm) or with different time incubation (for sorption kinetic study) in a 10 mL Teflon-lined
14
117
15   screw cap glass vial. 200 mg/L NaN$_3$ was used as a microbial inhibitor. The vials were placed on
16
118
17   a rotary shaker under dark condition at 150 rpm under 25±1°C until reaching sorption
18
119
19   equilibrium. The few-layered BP was then separated by centrifugation at 10,000 rpm for 30 min.
20
120
21   2 mL of the supernatant were removed and analyzed by UV. No Tyndall effect has been
22
121
23   observed (Figure S2) and no BP adsorption peak were found by UV-vis spectroscopy for the
24
122
25   supernatant (Figure S3), suggesting that the nanoparticles in solution were removed through
26
123
27   centrifugation. The amount of sorbed dyes on BP was calculated based on the difference between
28
124
29   initial and final aqueous concentrations. Experimental uncertainties were less than 1% of the
30
125
31   initial concentrations as evaluated by performing the sorption experiment in the absence of BP.
32
126
33   The concentration of PO$_3^{3-}$, PO$_4^{3-}$, P$_2$O$_7^{4-}$, and P$_3$O$_9^{3-}$ in the suspension before and after sorption
34
127
35   monitored by ion chromatography (Dinoex ICS-5000) did not elicit significant difference,
36
128
37   indicating the degradation of few-layered BP could be neglected during sorption.
38
129
39
40   Three sorption isotherm models, i.e. Langmuir model (LM), Freundlich model (FM), and
41
130
42   Dubinin-Ashtakhov model (DA), were used to fit sorption isotherms. They can be expressed as
43
131
44   follows:
45
132
46
47   LM: $Q_e = Q^0 K C_e / (1 + b C_e)$
48
133
49
50   FM: $Q_e = K_f C_e^n$
51
134
52
53   DA: $log Q_e = log Q^0 - (\varepsilon/E)^b$
54
135

6
55
56
57
58
59
60

136   where Q_e (mg/g) is the equilibrium sorbed concentration; C_e (mg/L) is the equilibrium solution

137   phase concentration; Q^0 (mg/g) is the maximum monolayer adsorption capacity; K is a constant

138   related to the molar heat of adsorption; K_f [(mg g^{-1})/(mg L^{-1})^n] is Freundlich affinity coefficient;

139   n is Freundlich exponential coefficient; ε (kJ mol^{-1}) = RTln(C_s/C_e) is the effective adsorption

140   potential; R [8.314 × 10^{-3} kJ (mol K)$^{-1}$] is the universal gas constant; T (K) is the absolute

141   temperature; E (kJ/mol) is the "correlating divisor" and b is the fitting parameter.

142   The separation factor (R_L) was used to examine the favorability of dyes sorption by BP. It can

143   be expressed as:

144       $R_L = 1/(1+KC_0)$

145   where K is the LM constant related to the molar heat of adsorption, C_0 (mg/L) is the initial

146   concentration of sorbate.

147   DA model based site energy frequency distribution F(E*) can be presented as below:[18]

148       $F(E^*) = \dfrac{ln10 \times b \times Q^0 \times E^{*(b-1)}}{E^b \times 10^{[(E^*/E)^b]}}$

149   where b is the fitting parameter of DA, E (kJ/mol) is the "correlating divisor".

150

151   Adsorption kinetics data were fitted by the pseudo-first order model (PFOM), pseudo-second

152   order model (PSOM) and the intraparticle diffusion model (IPDM), respectively. They can be

153   expressed as follows:

154   PFOM: $q_t = q_e(1 - e^{k_1 t})$

155   where q_t and q_e are the amount sorbed at time t and at equilibrium (mg/g); k_1 is the rate constant

156   of pseudo-first order sorption (1/h)

157   PSOM:

7

158    $$\frac{t}{q_t} = \frac{1}{k_2 q_e^2} + \frac{t}{q_e}$$

159    $$q_t = t/[(1/k_2 q_e^2) + (t/q_e)]$$

160   where q_t (mg/g) and q_e (mg/g) are the same as defined in PFOM; k_2 is the rate constant of

161   pseudo-second order sorption (g/mg/h); When t approach to 0, the initial sorption rate h (mg/g/h)

162   is:

163    $$h = k_2 q_e^2$$

164   IPDM: $q_t = k_i t^{1/2} + \theta$

165   where θ is the intercept of the linear portion of the plot, and k_i is the intraparticle diffusion rate

166   constant (mg/g/h$^{1/2}$).

167   The root mean square error of calibration (RMSEC) was used to evaluate the goodness of fit

168   for both sorption isotherm and kinetic models. It can be expressed as:

169    $$RMSEC = \sqrt{\frac{\sum_{i=1}^{n}(Y_i^{exp} - Y_i^{pred})^2}{n}}$$

170   where: Y_i^{exp} is the experimental value for the ith sample; Y_i^{pred} represents predicted value for the

171   ith sample; n is the number of samples.

172   **Computational methods**

173   A supercell containing 200 C atoms (a × b × c = 24.6 × 24.6 × 40 Å^3) and a supercell containing

174   192 P atoms (a × b × c = 26.47 × 26.45 × 40 Å^3) were used in the calculations. For either

175   adsorbent supercell, the distance of the axis perpendicular to graphene (GP) or black BP

176   direction was set as 40 Å, in order to avoid the interactions induced by periodic structures. For

177   either GP or BP, three adsorption orientations of MB were considered in the calculations, i.e.

178   standing with the S atom, standing with the N atom and lying. In the case of BP, for both the

8

179   armchair and the zigzag directions, three adsorption configurations of MB were calculated,

180   respectively.

181   Energy minimization of the adsorption configurations was performed based on density functional

182   theory (DFT) with the Dmol^3 program in Material Studio (Accelrys, San Diego, CA). The

183   exchange-correlation energy was calculated using a generalized gradient approximation (GGA)

184   method with the Perdew-Burke-Ernzerhof (PBE) formulation.[19] The DND double numerical

185   basis set, comparable to 6-31G* basis set, was used. A long range dispersion energy correction

186   was added by the local environment dependent approach by Tkatchenko and Scheffler (TS).[20] A

187   Fermi smearing of 0.006 Ha and a global orbital cutoff of 4 Å were used. The convergence

188   criteria was set as 1×10^{-5} Ha/atom for a self-consistent field tolerance, 2×10^{-5} Ha/atom for an

189   energy tolerance, 0.004 Ha/Å for a maximum force tolerance and 0.005 Å for a maximum

190   displacement tolerance. The geometry optimization process was conducted in the solvent (i.e.

191   water) simulated by a conductor-like screening model.[21, 22]

192   The adsorption energy ($E_{adsorption}$) and distortion energy ($E_{distortion}$) were calculated according to

193   Equations (1) and (2),

194    $E_{adsorption} = E_{complex} - (E_{MB} + E_{adsorbent})$ (1)

195    $E_{distortion} = E'_{adsorbent} - E_{adsorbent}$ (2)

196   where $E_{complex}$ stands for energy of energy minimized adsorption complex. E_{MB} and $E_{adsorbent}$ are

197   energies of individual MB and adsorbent, respectively. Then, a negative $E_{adsorption}$ value

198   represents the adsorption configuration is thermodynamically stable, while a positive $E_{adsorption}$

199   value means the adsorption configuration is thermodynamically unfavorable. $E'_{adsorbent}$ is energy

200   of the distorted adsorbent after adsorption. The distortion can be directly observed from the final

201   image. The distortion energy $E_{distortion}$ can quantitatively reflect the degree of distortion for the

202   BP nanosheets. A higher $E_{distortion}$ value means that the adsorbent experiences a more significant

203   distortion process. The distortion was caused completely by the attraction between MB and

204   adsorbent. No other external forces were added to the calculation system.

RESULTS AND DISCUSSION

206   Few-layered BP was successfully exfoliated and well dispersed by a facile, environmentally

207   friendly, and scalable ultrasonication technique without any organic solvents (**Figure 1**a). The

208   few-layered BP was (semi-)transparent, reflecting its 2D structure (Figure 1b). According to the

209   atomic force microscopy (AFM) images (Figure 1c), the as-exfoliated BP had an average

210   thickness of 5.89 ± 4.58 nm (Figure 1c and 1d), indicating their layer number was from 2 to 20.

211   The lateral size of few-layered BP was 158.0 ± 58.4 nm (Figure 1e). The average hydrodynamic

212   size in background solution (pH=7, 0.01 M Na^+, phosphorus buffer) increased to 716.9 ± 67.7

213   nm, probably attributed to the salt-induced aggregation of few-layered BP (Figure 1f). Two

214   characteristic peaks at 130.4 and 129.6 eV, corresponding to the binding energy of $2P^{1/2}$ and $2P^{3/2}$

215   respectively, were detected by X-ray photoelectron spectroscopy (XPS) analysis (Figure 1g).[23, 24]

216   The small peak at 133.8 eV was probably due to the existence of oxidized phosphorus, which

217   could give an explanation to its negative zeta potential of -29.6 ± 5.03 mV (Figure 1i). Three

218   prominent peaks, i.e. A^1_g (out-of-plane phonon modes, assigned to 364 cm^{-1}), B_{2g} and A^2_g (in-

219   plane modes, assigned to 440 and 468 cm^{-1}), characterized by Raman spectroscopy, were

220   consistent with the previous report,[24] further confirming the successful exfoliation and dispersion

221   of BP (Figure 1h). The intensity ratio of A^1_g/ A^2_g was 1.189, greater than 0.6, illustrating the

222   basal planes of BP nanosheets to be slightly or un-oxidized.[25]

223   Sorption experiments were performed using a batch equilibration technique at 25±1 °C under

224   anaerobic condition. No new peaks of both dyes in the UV-vis spectra and HPLC spectra

225   occurred during the entire sorption procedure with different initial concentrations and times,

226   indicating negligible degradation of dyes (Figure S3, Supplementary Information). Few-layered

227   BP showed excellent removal efficiencies for MB and CR **(Figure 2**a, bottom photos). Sorption

228   isotherms were fit to three isotherm models, i.e. Langmuir model (LM), Freundlich model (FM),

229   and Dubinin-Ashtakhov model (DA) (Figure 2a and Table S1). For both dyes, LM model had a

230   better fit than FM, suggesting the surface of BP is relatively homogeneous.[26] This was consistent

231   with the characterization results that BP was well exfoliated and dispersed with only slight

232   oxidation on the surface. The dimensionless separation factor R_L can help to evaluate the

233   favorability of the sorption: (i) unfavorable when $R_L > 1$, (ii) favorable when $R_L < 1$, and (iii)

234   irreversible when $R_L = 0$.[27] The plotted R_L value ranged from 0-1 for all the studied

235   concentrations (Figure S4, Supplementary Information), indicating both MB and CR sorption on

236   BP was favorable. According to the higher values of adjusted correlation coefficients (r^2_{adj}),

237   which has already overcome the effect of over-parameterization, and the lower value of RMSEC,

238   DA model had a better fit than LM and FM models for both dyes (Table S1, Supplementary

239   Information). The sorption capacity obtained from DA was 1232 ± 283 mg/g and 230 ± 9 mg/g

240   for MB and CR, respectively (Table S1, Supplementary Information). The sorption capacity of

241   few-layered BP in our work is higher than that of most adsorbents listed (**Table 1**), except

242   graphene oxide (GO) for CR, indicating the few-layered BP a potential adsorbent for the IOC

243   removal.

244   To find out why BP has such high sorption capacities, we first investigated the interactions

245   between BP and the dyes. Considering the cationic property of MB and the negative surface

246   charge (-29.6 ± 5.03 mV) of few-layered BP in the background solution, the electrostatic

247   interaction was expected to take place. Previous study also demonstrated the electrostatic

248   interaction should be the dominant mechanism for DOX sorption onto BP.[17] Since BP also had a

249   high sorption capability for negatively charged CR, there must be additional mechanisms besides

250   electrostatic interaction. The few-layered BP surface has an average contact angle of ~57°,

251   indicating that the hydrophobicity of BP is between graphene (GP, ~90°) and GO (~27°).[44]

252   Therefore, hydrophobic interaction needs to be included. No significant differences have been

253   detected for both dyes at different Na^+ levels (0.001M, 0.005M and 0.01M) at initial solute

254   concentration of 50 and 500 mg/L (Figure S5), suggesting ion exchange mechanism was

255   negligible. However, both electrostatic and hydrophobic interactions are common between the

256   IOCs and other adsorbents, such as GP, activated carbon, and biochars. The sorption site energy

257   distributions of both dyes on few-layered BP were among 0~30 kJ/mol (Figure 2b), which was

258   also similar to the IOCs sorption on carbonaceous materials.[45, 46] Thus, there should be other

259   undiscovered mechanisms responsible for the higher sorption capacity of BP.

260   We then calculated the maximum theoretical specific surface area of single layered BP. The

261   surface area (S_h – Figure 2c) of one armchair unit at one side is:

262       $S_h = 2S_1 + S_2 = 2d^2_{1p-p}Sin(96.3°/2)Cos(96.3°/2)+2\ d_{1p-p}Sin(96.3°/2)\ d_{2p-p}$

263       $= 1.23513 \times 10^{-19}\ m^2$ (3)

264   S_h corresponds to two phosphorus atoms, whose weight is equal to one armchair unit of BP.

265   Taking the atomic weight of phosphorus ($M_P = 30.97$ g/mol) and the Avogadro number ($N =$

266    $6.023 \times 10^{23}\ mol^{-1}$) into account, the one unit weight can be expressed as:

267       $W_h = (2M_P/N) = 1.028562 \times 10^{-22}\ g$ (4)

268   Combining equations (3) and (4), the specific surface area (SSA) of a single BP layer can be

269   obtained:

270    $SSA = 2S_h / W_h = 2400 \text{ m}^2/\text{g}$ (5)

271   The maximum theoretical specific surface area of single layered BP is higher than that of

272   carbon nanotubes (1315 m^2/g), and is comparable to that of GP (2630 m^2/g).[47] The calculated

273   SSA can only tell that few-layered BP has a comparable sorption capacity with GP, but it still

274   cannot explain why it has a higher sorption capacity than GP and other adsorbents.

275   Sorption kinetic study was further conducted in order to disclose the underlying mechanism.

276   The sorption equilibrium time was 60 h for 100 mg/L MB, while CR took a longer time (90 h) to

277   reach equilibrium (Figure 2d). Among the three sorption kinetic models, i.e. pseudo-first order

278   model (PFOM), pseudo-second order model (PSOM), and intraparticle diffusion model (IPDM),

279   only IPDM could well fit the sorption data (r^2 is 0.947 and 0.984 for MB and CR, respectively,

280   RMSEC was 13.403 and 4.973 for MB and CR, respectively, Figure 2d and Table S2),

281   suggesting the intraparticle diffusion mechanism was involved in both sorption processes.[48] The

282   IPDM parameter θ of MB sorption was 47.10±7.41, demonstrating intermediate adsorption

283   profile.[49] While for CR, θ was 6.42±2.48, approaching to 0, suggesting the intraparticle diffusion

284   was the rate-controlling step. Electrostatic attraction/repulsion should be the reason for the

285   different θ values: electrostatic attraction between the positively charged MB and negatively

286   charged BP surface; electrostatic repulsion between both negatively charged CR and BP surface.

287   Therefore, CR needs to overcome electrostatic repulsion and desolvation to adsorb onto BP

288   surface, in comparison, MB only needs to compensate for desolvation. In addition, CR was twice

289   the steric size than MB, which means that CR needs to overcome more steric energy for sorption.

290   The difference in electrostatic attraction/repulsion combined with the steric effects led MB to

291   have lower sorption distribution energy sites than CR (Figure 2b). Again, since the intraparticle

292   diffusion has also been reported in IOCs sorption on GP and other adsorbents.[48-50] we still cannot

293   answer the question why few-layered BP has such high sorption capacities.

294   Previous study on the sorption of organic compounds on GP and GO nanosheets revealed that

295   after loading with organic molecules, the conformation and aggregation of GP and GO

296   nanosheets dramatically changed.[51] Thus, AFM and TEM images were taken to compare the

297   morphological changes of the few-layered BP before and after sorption (**Figures 3**). To our

298   surprise, unusual wrinkle formation was observed after sorption. By adjusting the initial

299   concentration of dyes, the average thickness of few-layered BP slightly decreased from 5.89 nm

300   to 5.71 nm and 3.99 nm for 50 mg/L and 500 mg/L MB (equilibrium concentration 25 mg/L and

301   409 mg/L), respectively (Figure 3), and to 3.43 nm and 2.71 nm for 50 mg/L and 500 mg/L CR

302   (equilibrium concentration 25 mg/L and 474 mg/L), respectively (Figure S6). Previous study

303   indicated that the deformation of BP can be accomplished under a single strain condition, to

304   control anisotropic free-carrier mobility[52] and to modify gap size of BP.[53] Hence, we

305   hypothesized that the deformation of BP, i.e. wrinkle formation, could be generated from the

306   interactions between few-layered BP and the ionic dyes, which created new sorption sites

307   between layers, then further induced sorption (Figure 4). It is this wrinkle-induced sorption to

308   endow the few-layered BP with an extremely high sorption capacity.

309   The wrinkle formation was further verified by theoretically comparing the sorption of MB on

310   BP to that on GP via DFT calculation (**Table 2**, **Figure 5 and Figure S7**). The adsorption

311   energies varied significantly for MB sorption on BP with different sorption geometry

312   configurations. Two horizontal sorption geometry configurations (BP1 and BP2) were

313   thermodynamically favorable, with adsorption energy -1.03 eV and -0.90 eV, respectively (Table

314 2). The adsorption energy was a bit lower than that of GP1 (-1.60 eV), meaning that the affinity

315 of MB to GP is higher than that to BP. The distortion energy of adsorbents, however, shows that

316 BP is much easier to bend during adsorption than GP. For the favorable configurations, the

317 distortion energy of BP is 1.67 - 3.67 times higher than that of GP. This character of BP could be

318 completely attributed to its puckered structure, making it not as rigid as graphene, and easier to

319 form wrinkles. It is noteworthy that DFT calculation is on the molecular level, that is to say,

320 wrinkle formation occurred within the whole concentration range. However, comparative

321 sorption study between graphene and BP showed that it was not until 18.3 mg/L (for MB) and

322 66.3 mg/L (for CR), respectively, that wrinkle formation became dominant (Figure 6). In

323 addition, it took 60 h for 100 mg/L MB, and 90 h for CR to reach sorption equilibrium,

324 indicating that

CONCLUSION

326 In summary, we revealed few-layered BP as a new efficient adsorbent, with high adsorption

327 capacities for both cationic MB (1232 ± 283 mg/g) and anionic CR (230 ± 9 mg/g), one of the

328 highest capabilities ever reported. The wrinkle-induced mechanism was observed and verified to

329 account for the high adsorption capacities. This highly effective adsorbent may become a

330 promising candidate to remove IOCs from aqueous solution in the future environmental

331 application. It is noted that due to the unstable nature of BP, currently the sorption experiment

332 was conducted under oxygen free condition, which is far away from its realistic applications.

333 Further studies are required to enhance BP stability, to adsorb more types of pollutants, and

334 finally to develop an economic practical technology for waste water treatment. Our findings on

335 the wrinkle-induced high sorption mechanism provide a new strategy for nano-adsorbent

336 designing.

15

Supplementary Information

Additional information for Chemical structures of methylene blue and congo red; UV-vis spectra of MB and CR during sorption varied with time and initial concentration; HPLC spectra of MB and CR after sorption. Results of LM, FM, and DA models fitted sorption data of two dyes by few-layered BP; Variation of separation factor RL with dyes' initial concentration C_0; Comparison of amount sorption of two dyes at different Na^+ concentration levels at initial concentration of 50 and 500 mg/L respectively; Maximum sorption capacities of MB and CR on various sorbents; Results of PFOM, PSOM, and IPDM fitted with sorption kinetic data of two dyes by few-layered BP; TEM images (a-c), AFM images and statistical analysis of the thickness of few-layered BP before and after sorption at the initial CR concentration of 50 mg/L and 500 mg/L; Initial and energy minimized configurations of adsorption complex, i.e. MB adsorbed on graphene (GP2-3) and phosphorene (BP4-6) is provided in the ESI file.

AUTHOR INFORMATION

Corresponding Author

*E-mail: zhangxuejiao@iae.ac.cn (Xuejiao Zhang); syzhang@iae.ac.cn (Siyu Zhang); bx@umass.edu （Baoshan Xing）

Author Contributions

† These authors contributed equally.

Notes

ACKNOWLEDGMENT

364   **REFERENCES**

365   1 K. L. Howdeshell, A. K. Hotchkiss, K. A. Thayer, J. G. Vandenbergh and F. S. Vom Saal,
366   Environmental toxins: exposure to bisphenol A advances puberty, *Nature*, 1999**, 401**, 763.
367   2 W. Witte, Medical consequences of antibiotic use in agriculture, *Science*, 1998**, 279**, 996-997.
368   3 D. Ferber, Antibiotic resistance - WHO advises kicking the livestock antibiotic habit, *Science*,
369   2003, **301**, 1027-1027.
370   4 F. Xiao and J. J. Pignatello, Pi(+)-pi interactions between (hetero)aromatic amine cations and
371   the graphitic surfaces of pyrogenic carbonaceous materials, *Environ. Sci. Technol.*, 2015, **49**,
372   906-914.
373   5 G. X. Zhao, L. Jiang, Y. D. He, J. X. Li, H. L. Dong, X. K. Wang and W. P. Hu, Sulfonated
374   graphene for persistent aromatic pollutant management, *Adv. Mater.*, 2011, **23**(34), 3959-3963.
375   6 G. Cornelissen, Ö. Gustafsson, T. D. Bucheli, M. T. O. Jonker, A. A. Koelmans and P. C. M.
376   van Noort, Extensive Sorption of Organic Compounds to Black Carbon, Coal, and Kerogen in
377   Sediments and Soils: Mechanisms and Consequences for Distribution, Bioaccumulation, and
378   Biodegradation, *Environ. Sci. Technol.*, 2005, **39**, 6881-6895.
379   7 K. Yang, W. Wu, Q. Jing and L. Zhu, Aqueous Adsorption of Aniline, Phenol, and their
380   Substitutes by Multi-Walled Carbon Nanotubes, *Environ. Sci. Technol.*, 2008, **42**, 7931-7936.
381   8 W. Lei, G. Liu, J. Zhang and M. Liu, Black phosphorus nanostructures: recent advances in
382   hybridization, doping and functionalization, *Chem. Soc. Rev.*, 2017, 3492-3509.
383   9 D. Hanlon, C. Backes, E. Doherty, C. S. Cucinotta, N. C. Berner, C. Boland, K. Lee, A.
384   Harvey, Lynch, P.; Gholamvand, Z.; Zhang, S.; Wang, K.; Moynihan, G.; Pokle, A.; Ramasse, Q.
385   M.; N. McEvoy, W. J. Blau, J. Wang, G. Abellan, F. Hauke, A. Hirsch, S. Sanvito, D. D.
386   O'Regan, G. S. Duesberg, V. Nicolosi and J. N. Coleman, Liquid exfoliation of solvent-
387   stabilized few-layer black phosphorus for applications beyond electronics, *Nat. Commun.*, 2015,
388   **6**.
389   10 F. Xia, H. Wang and Y. Jia, Rediscovering black phosphorus as an anisotropic layered
390   material for optoelectronics and electronics, *Nat. Commun.*, 2014, **5**, 4458-4464.
391   11 M. Buscema, D. J. Groenendijk, S. I. Blanter, G. A. Steele, H. S. J. van der Zant and A.
392   Castellanos-Gomez, Fast and Broadband Photoresponse of Few-Layer Black Phosphorus Field-
393   Effect Transistors, *Nano Lett.*, 2014, **14**, 3347-3352.

12 M. J. Rodrigues, C. J. de Matos, Y. W. Ho, H. Peixoto, R. E. de Oliveira, H. Y. Wu, A. H. C. Neto and J. Viana‑Gomes, Resonantly increased optical frequency conversion in atomically thin black phosphorus, *Adv. Mater.*, 2016, **28**, 10693-10700.

13 Z. Guo, H. Zhang, S. Lu, Z. Wang, S. Tang, J. Shao, Z. Sun, H. Xie, H. Wang, X.-F. Yu and P. K. Chu, From Black Phosphorus to Phosphorene: Basic Solvent Exfoliation, Evolution of Raman Scattering, and Applications to Ultrafast Photonics, *Adv. Funct. Mater.*, 2015, **25**, 6996-7002.

14 C. Sun, L. Wen, J. Zeng, Y. Wang, Q. Sun, L. Deng, C. Zhao and Z. Li, One-pot solventless preparation of PEGylated black phosphorus nanoparticles for photoacoustic imaging and photothermal therapy of cancer, *Biomaterials*, 2016, **91**, 81-89.

15 H. Wang, X. Yang, W. Shao, S. Chen, J. Xie, X. Zhang, J. Wang and Y. Xie, Ultrathin black phosphorus nanosheets for efficient singlet oxygen generation, *J. Am. Chem. Soc.*, 2015, **137**, 11376-11382.

16 W. Tao, X. Zhu, X. Yu, X. Zeng, Q. Xiao, X. Zhang, X. Ji, X. Wang, J. Shi and H. Zhang, Black phosphorus nanosheets as a robust delivery platform for cancer theranostics, *Adv. Mater.*, 2017, **29**.

17 W. Chen, J. Ouyang, H. Liu, M. Chen, K. Zeng, J. Sheng, Z. Liu, Y. Han, L. Wang and J. Li, Black Phosphorus Nanosheet‑Based Drug Delivery System for Synergistic Photodynamic/Photothermal/Chemotherapy of Cancer, *Adv. Mater.*, 2017, **29**.

18 X. F. Shen, X. Y. Guo, M. Zhang, S. Tao and X. L. Wang, Sorption mechanisms of organic compounds by carbonaceous materials: site energy distribution consideration, *Environ. Sci. Technol.*, 2015, **49**, 4894-4902.

19 J. P. Perdew, K. Burke and M. Ernzerhof, Generalized gradient approximation made simple, *Phys. Rev. Lett.*, 1996, **77**, 3865.

20 A. Tkatchenko and M. Scheffler, Accurate molecular van der Waals interactions from ground-state electron density and free-atom reference data, *Phys. Rev. Lett.*, 2009, **102**, 073005.

21 A. Klamt and G. Schüürmann, COSMO: a new approach to dielectric screening in solvents with explicit expressions for the screening energy and its gradient, *J. Chem. Soc. Perk. T. 2*, 1993, 799-805.

22 B. Delley, The conductor-like screening model for polymers and surfaces, *Mol. Simulat.*, 2006, **32**, 117-123.

23 J. Kang, J. D. Wood, S. A. Wells, J.-H. Lee, X. Liu, K.-S. Chen and M. C. Hersam, Solvent Exfoliation of Electronic-Grade, Two-Dimensional Black Phosphorus, *ACS Nano*, 2015, **9**, 3596-3604.

24 X. Zhang, Z. Zhang, S. Zhang, D. Li, W. Ma, C. Ma, F. Wu, Q. Zhao, Q. Yan and B. Xing, Size Effect on the Cytotoxicity of Layered Black Phosphorus and Underlying Mechanisms, *Small*, 2017, **13**, 1701210.

25 A. Favron, E. Gaufres, F. Fossard, A.-L. Phaneuf-Lheureux, N. Y. W. Tang, P. L. Levesque, A. Loiseau, R. Leonelli, S. Francoeur and R. Martel, Photooxidation and quantum confinement effects in exfoliated black phosphorus, *Nat. Mater.*, 2015, **14**, 826-832.

26 T. Liu, Y. Li, Q. Du, J. Sun, Y. Jiao, G. Yang, Z. Wang, Y. Xia, W. Zhang, K. Wang, H. Zhu and D. Wu, Adsorption of methylene blue from aqueous solution by graphene, *Colloids Surf. B. Biointerfaces*, 2012, **90**, 197-203.

27 S. Debnath, A. Maity and K. Pillay, Impact of process parameters on removal of Congo red by graphene oxide from aqueous solution, *J. Environ. Chem. Eng.*, 2014, **2**, 260-272.

28 G. K. Ramesha, A. Vijaya Kumara, H. B. Muralidhara and S. Sampath, , Graphene and graphene oxide as effective adsorbents toward anionic and cationic dyes, *J. Colloid Interface Sci.*, 2011, **361**(1), 270-277.

29 T. Liu, Y. Li, Q. Du, J. Sun, Y. Jiao, G. Yang, Z. Wang, Y. Xia, W. Zhang, K. Wang, H. Zhu and D. Wu, Adsorption of methylene blue from aqueous solution by graphene, *Colloids Surf. B. Biointerfaces*, 2012, **90**, 197-203.

30 H. Yan, X. Tao, Z. Yang, K. Li, H. Yang, A. Li and R.Cheng, Effects of the oxidation degree of graphene oxide on the adsorption of methylene blue, *J. Hazard. Mater.*, 2014, **268**, 191-198.

31 K. V. Kumar and S. Sivanesan, Equilibrium data, isotherm parameters and process design for partial and complete isotherm of methylene blue onto activated carbon, *J. Hazard. Mater.*, 2006, **134**(1), 237-244.

32 J. Ma, F. Yu, L. Zhou, L. Jin, M. Yang, J. Luan, Y. Tang, H. Fan, Z. Yuan and J. Chen, Enhanced adsorptive removal of methyl orange and methylene blue from aqueous solution by alkali-activated multiwalled carbon nanotubes, *ACS Appl. Mater. Inter.*, 2012, **4** (11), 5749-5760.

33 F. Liu,; S. Chung, G. Oh and T. S. Seo, Three-dimensional graphene oxide nanostructure for fast and efficient water-soluble dye removal, *ACS Appl. Mater. Inter.*, 2012, **4**(2), 922-927.

34 S.-T. Yang, S. Chen, Y. Chang, A. Cao, Y. Liu and H. Wang, Removal of methylene blue from aqueous solution by graphene oxide, J. *Colloid Interface Sci.*, 2011, **359**(1), 24-29.

35 L. Zhang, Y. Zhang, L. Yang, X. Jiang and Q. Yang, A rapid method for the removal of Methyl blue dye from wastewater by magnetic nanoparticles Mn-ferrites, *Desalin. Water Treat.*, 2015, **54**(8), 2259-2269.

36 X. Rong, F. Qiu, J. Qin, H. Zhao, J. Yan and D. Yang, A facile hydrothermal synthesis, adsorption kinetics and isotherms to Congo Red azo-dye from aqueous solution of NiO/graphene nanosheets adsorbent, *J. Ind. Eng. Chem.*, 2015, **26**, 354-363.

37 Y. Yao, S. Miao, S. Liu, L. P. Ma, H. Sun and S. Wang, Synthesis, characterization, and adsorption properties of magnetic Fe3O4@graphene nanocomposite, *Chem. Eng. J.*, 2012, **184**, 326-332.

38 Q. Du, J. Sun, Y. Li, X. Yang, X. Wang, Z. Wang and L. Xia, Highly enhanced adsorption of congo red onto graphene oxide/chitosan fibers by wet-chemical etching off silica nanoparticles, *Chem. Eng. J.*, 2014, **245**, 99-106.

39 E. Bulut, M. Özacar and İ. A. Şengil, Equilibrium and kinetic data and process design for adsorption of Congo Red onto bentonite, *J. Hazard. Mater.*, 2008, **154**(1), 613-622.

40 L. Wang and A.Wang, Adsorption characteristics of Congo Red onto the chitosan/montmorillonite nanocomposite, *J. Hazard. Mater.*, 2007, **147**(3), 979-985.

41 C. Namasivayam and D. J. S. E. Arasi, Removal of congo red from wastewater by adsorption onto waste red mud, *Chemosphere* 1997, **34**(2), 401-417.

42 V. Vimonses, S. Lei, B. Jin, C. W. K. Chow and C. Saint, Kinetic study and equilibrium isotherm analysis of Congo Red adsorption by clay materials, *Chem. Eng. J.*, 2009, **148**(2), 354-364.

43 L. Lian, L. Guo and C. Guo, Adsorption of Congo red from aqueous solutions onto Ca-bentonite, *J. Hazard. Mater.*, 2009, **161**(1), 126-131.

44 J. Kang, S. A. Wells, J. D. Wood, J.-H. Lee, X. Liu, C. R. Ryder, J. Zhu, J. R. Guest, C. A. Husko and M. C. Hersam, Stable aqueous dispersions of optically and electronically active phosphorene, *Proc. Natl. Acad. Sci. U.S.A.*, 2016, **113**, 11688-11693.

45 M. C. Carter, J. E. Kilduff and W. J. Weber, Site Energy Distribution Analysis of Preloaded Adsorbents, *Environ. Sci. Technol.*, 1995, **29**, 1773-1780.

46 X. F. Shen, X. Y. Guo, M. Zhang, S. Tao and X. L. Wang, Sorption mechanisms of organic compounds by carbonaceous materials: site energy distribution consideration, *Environ. Sci. Technol.*, 2015, **49**, 4894-4902.

47 A. Peigney, C. Laurent, E. Flahaut, R. R. Bacsa and A. Rousset, Specific surface area of carbon nanotubes and bundles of carbon nanotubes, *Carbon*, 2001, **39**, 507-514.

48 Q. Yu, R. Zhang, S. Deng, J. Huang and G. Yu, Sorption of perfluorooctane sulfonate and perfluorooctanoate on activated carbons and resin: Kinetic and isotherm study, *Water Res.*, 2009, **43**, 1150-1158.

49 A. E. Ofomaja, Kinetic study and sorption mechanism of methylene blue and methyl violet onto mansonia (Mansonia altissima) wood sawdust, *Chem. Eng. J.*, 2008, 143, 85-95.

50 H. Yan, X. Tao, Z. Yang, K. Li, H. Yang, A. Li and R.Cheng, Effects of the oxidation degree of graphene oxide on the adsorption of methylene blue, *J. Hazard. Mater.*, 2014, **268**, 191-198.

51 J. Wang, Z. Chen and B.Chen, Adsorption of Polycyclic Aromatic Hydrocarbons by Graphene and Graphene Oxide Nanosheets, *Environ. Sci. Technol.*, 2014, **48**, 4817-4825.

52 R. Fei and L.Yang, Strain-Engineering the Anisotropic Electrical Conductance of Few-Layer Black Phosphorus, *Nano Lett.*, 2014, **14**, 2884-2889.

53 A. S. Rodin, A. Carvalho and A. H. Castro Neto, Strain-Induced Gap Modification in Black Phosphorus, *Phys. Rev. Lett.*, 2014, **112**, 176801.

517
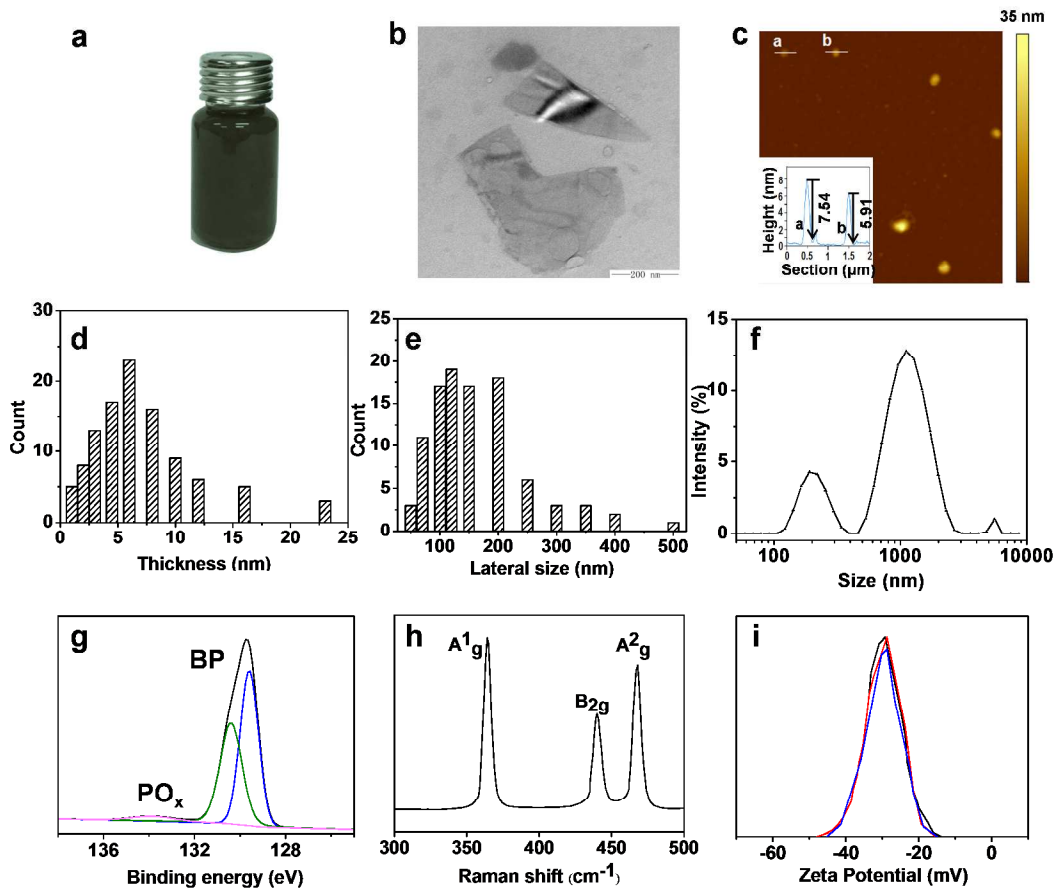
Figure 1. Characterizations of few-layered BP. (a) Photograph of the as-exfoliated few-layered BP dispersions in Milli-pore water; (b) Transmission electron microscopy (TEM) images and (c)AFM images of few-layered BP (c); Statistical analysis of the thickness (d) and lateral size (e) of 100 pieces of few-layered BP measured by AFM; (f) Size distributions of few-layered BP in background solution by dynamic light scattering (DLS) measurements; (g) XPS spectra and (h) Raman spectra of the as-exfoliated few-layered BP; (i) Zeta potential of few-layered BP in background solution.

524
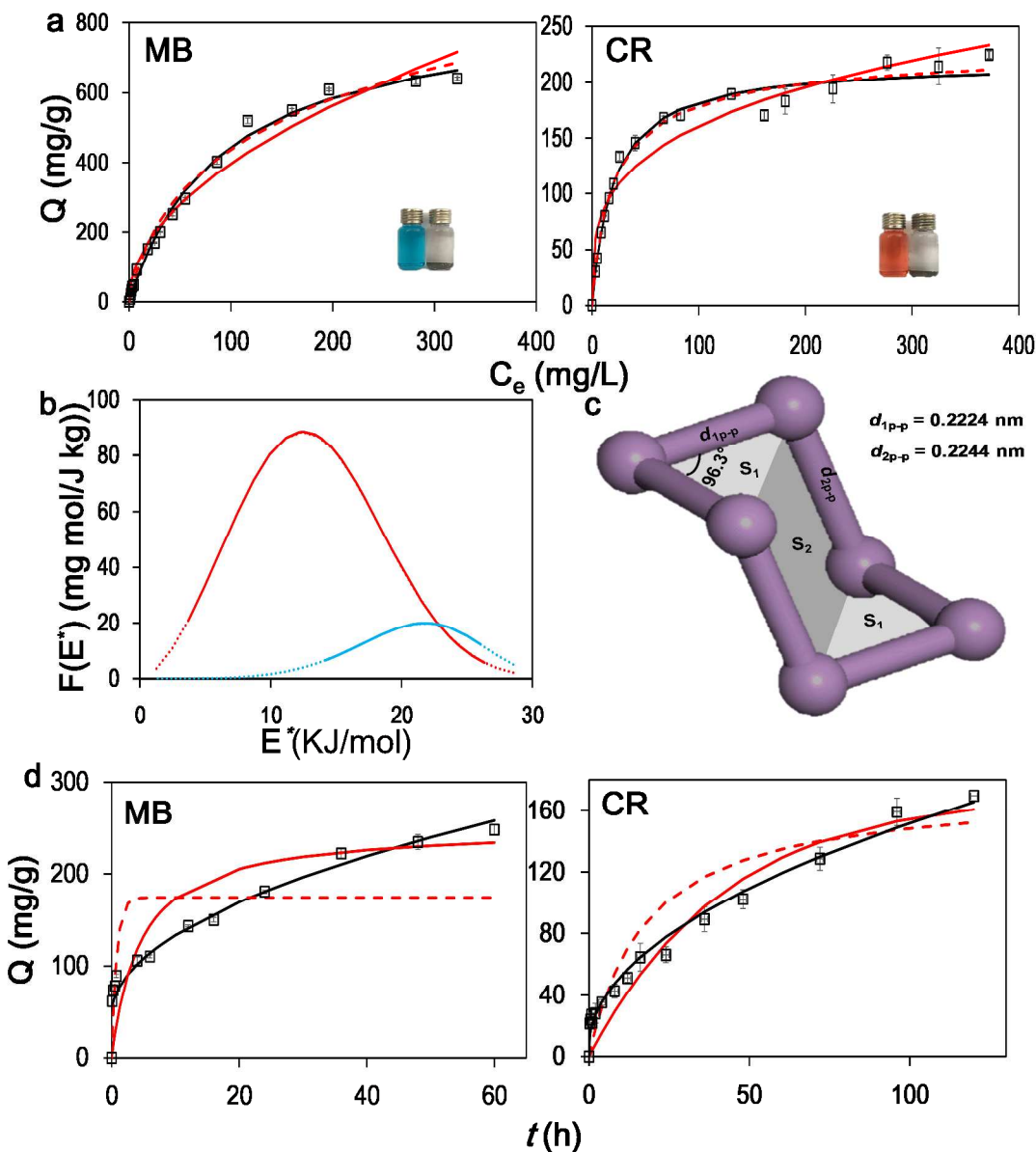
Figure 2. Mechanistic study of MB and CR sorption on few-layered BP. **(**a) Sorption isotherms of MB and CR fitted with Langmuir (black full line), Freundlich (red full line) and Dubinin-Ashtaklov (red dash line) models. Error bars represent the standard deviation of three replicates. Photos at the right bottom represent 10 mg/L dyes before and after sorption. (b) The DA isotherm model-based site energy distributions of two dyes on few-layered BP. The curves (red for MB, and blue for CR) in solid lines represent the site energy distributions in the experimental data range and those in dotted lines stand for the sites beyond the experimental data range. (c) Schematic representation of the structural armchair unit within monolayer BP. (d) Sorption kinetics of 100 mg/L dyes on few-layered BP fitted with PFOM (red dash line), PSOM (red full line), and IPDM (black full line).
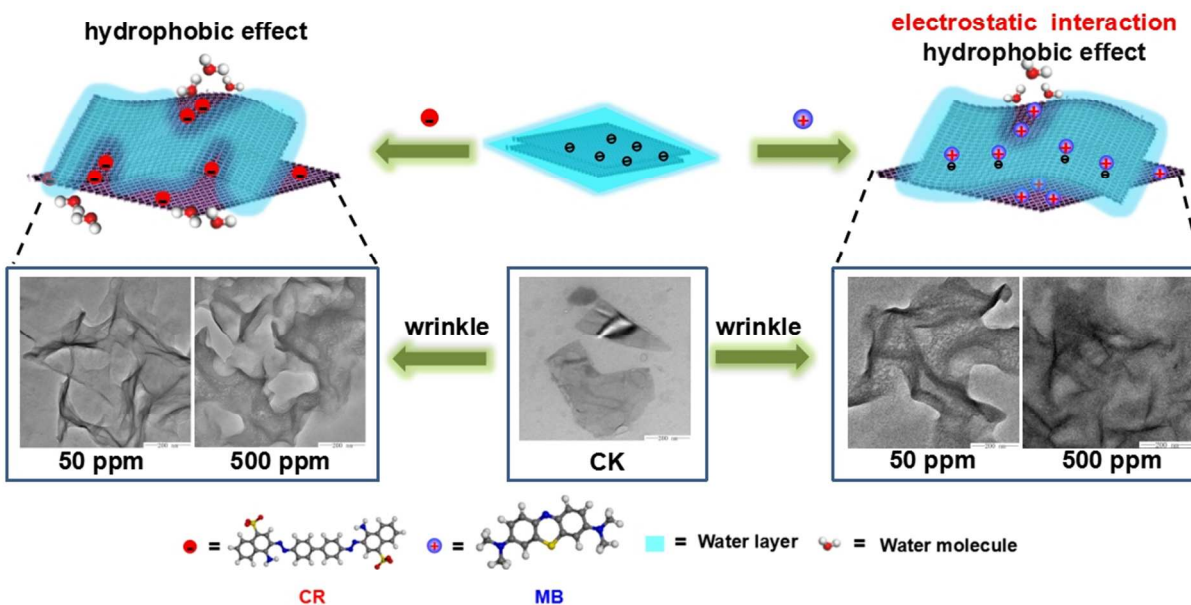
537
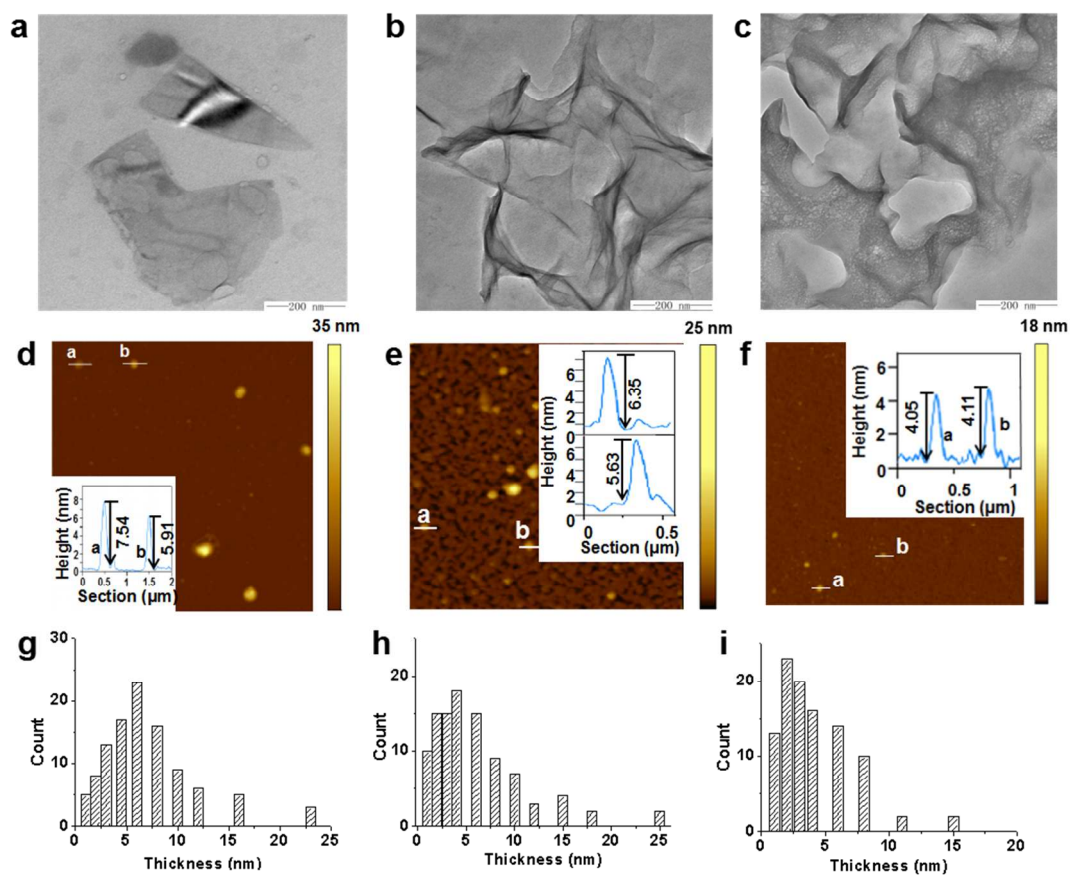
538
539
540 **Figure 3.** TEM images (a-c), AFM images (d-f), and statistical analysis of the thickness (g-i) of few-
541 layered BP before (a, d, and g) and after sorption at the initial MB concentration of 50 mg/L (b, e, and h)
542 and 500 mg/L (c, f, and i).

543

544

Figure 4. Schematic diagrams for sorption mechanisms of IOCs on BP. The wrinkle formation could be generated from the interactions between few-layered BP and the ionic dyes, which created new sorption sites between layers.
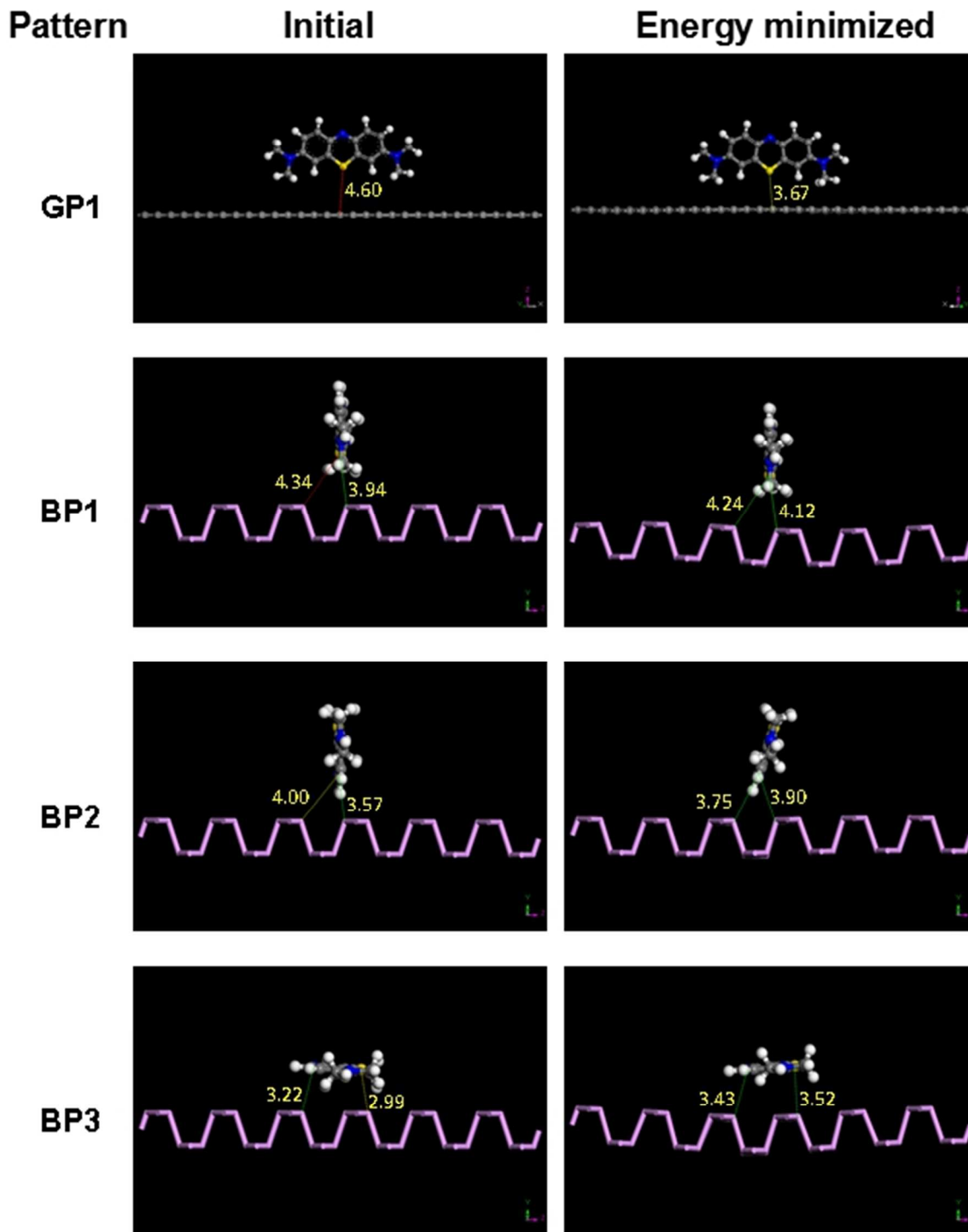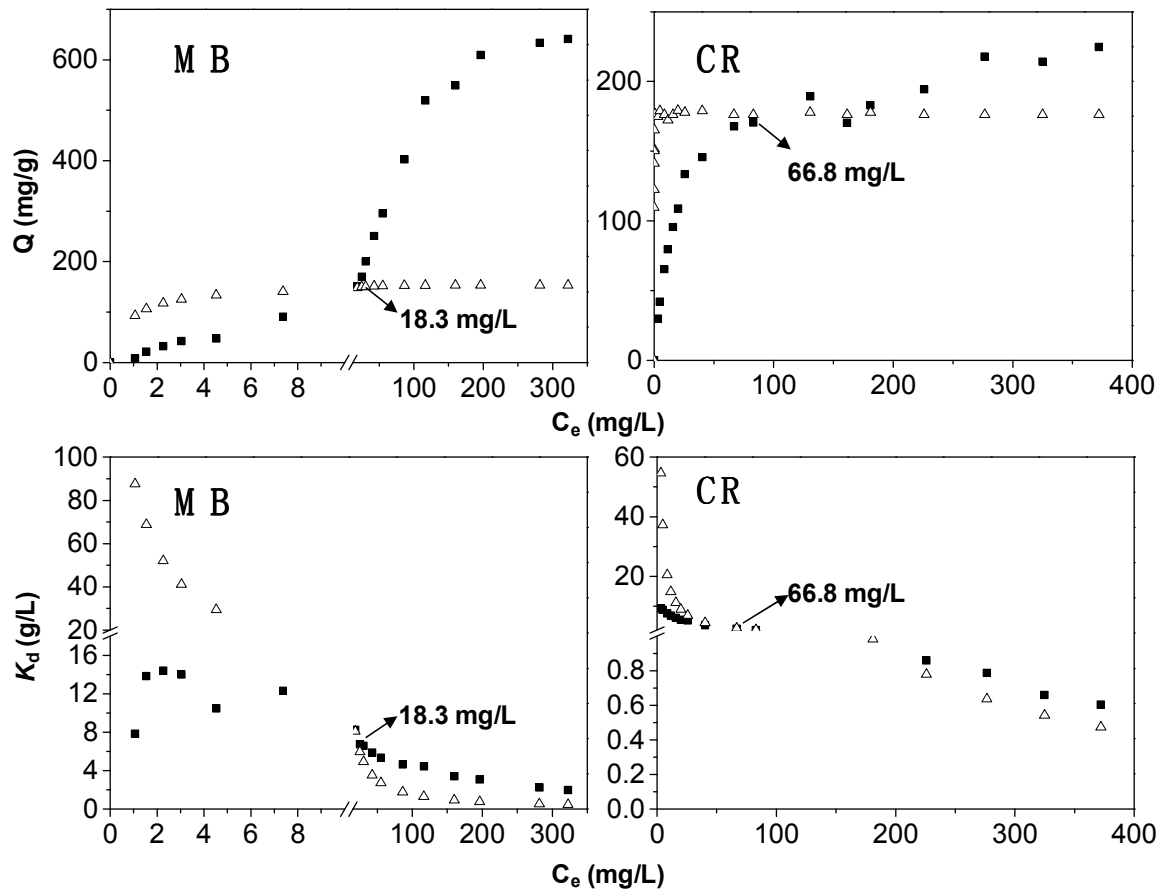
Figure 5. Intial (left panel) and energy minimized (right panel) configurations of adsorption complex, the most favorable cases: MB adsored on graphene (GP1) and phosphorene (BP1-3) (Dark gray balls: C atoms; Light gray balls: H atoms; blue balls: N atoms; yellow balls: S atoms; Pink balls: P atoms; Unit for distance is Å)

Figure 6. Comparative study of sorption amount Q and sorption coefficient K_d between two dyes sorption on BP (■) and GP (△).

583   **Table 1.** Maximum sorption capacities of MB and CR on various sorbents.

584

Chemicals	adsorbent	Maximum sorption capacity (mg/g)	Ref.
MB	GP and GO	17.3	28
	GP	153.85	29
	GP and GO	41.67-598.8	30
	activated carbon	400	31
	alkali-activated multiwalled carbon nanotubes	399	32
	threedimensional (3D) GO sponge	397	33
	GO	714	34
	$MnFe_2O_4$ nanoparticles	148.04	35
	few-layered BP	1232±283	This work
CR	NiO/GP nanosheets	123.89	36
	Magnetic Fe_3O_4@GP nanocomposite	45.27	37
	GP oxide/chitosan/silica fibers	294.12	38
	bentonite	158.7	39
	chitosan/montmorillonite nanocomposite	96.62	40
	red mud	4.05	41
	Kaolin	5.44	42
	Ca-bentonite	107.41	43
	few-layered BP	230±8.97	This work

585

586

587

588 **Table 2**. DFT calculated energies for individuals and adsorption complexes (GP1-3 and BP1-6),
589 adsorption energies ($E_{adsorption}$) and distortion energies of the adsorbents ($E_{distortion}$).

Pattern	E, hartree	$E_{adsorption}$, eV	$E_{distortion}$, eV
MB	-1181.9500	-	-
GP	-7617.2588	-	-
BP	-65518.1244	-	-
GP1	-8799.2676	-1.60	0.03
GP2	-8799.2180	-0.25	0.02
GP3	-8799.2115	-0.07	0.06
BP1	-66700.1121	-1.03	0.11
BP2	-66700.1077	-0.90	0.05
BP3	-66700.0660	0.23	0.12
BP4	-66700.0726	0.05	0.04
BP5	-66700.0708	0.10	0.09
BP6	-66700.0705	0.11	0.02

590
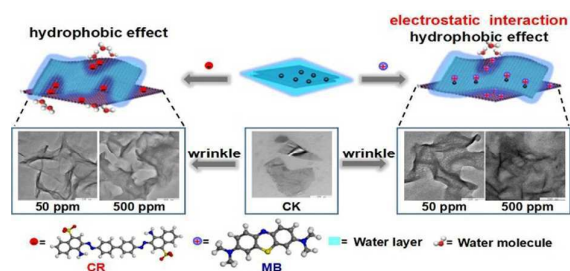
Wrinkle-induced high sorption makes few-layered black phosphorus a superior adsorbent for both cationic and anionic organic compounds.